Full Length Article

# Boron nanoparticles (BNPs) produced by ns-laser ablation in water: synthesis and characterization

Marcella Dell'Aglio [a,*], Alessandro De Giacomo [b], Daniela Manno [c,d], Antonia Mallardi [e], Chiara Provenzano [f], Marcella Marra [c], Francesco Nocito [b], Antonio Serra [c,d], Gianluca Quarta [c,d,g], Anna Paola Caricato [c,d]

[a] CNR-IFN (National Research Council - Institute for photonics and nanotechnologies), c/o Physics Department, University of Bari, Via Amendola 173, 70126, Bari, Italy
[b] Department of Chemistry, University of Bari, Via Orabona 4, 70125, Bari, Italy
[c] Department of Mathematics and Physics "E. De Giorgi" University of Salento, via per Arnesano, km 1, 73100, Lecce, Italy
[d] National Institute of Nuclear Physics (INFN-Le) at the Department of Mathematics and Physics "E. De Giorgi," University of Salento, via per Arnesano, km 1, 73100, Lecce, Italy
[e] CNR-IPCF, Institute for Chemical-Physical Processes, c/o Chemistry Department, University of Bari, Via Orabona 4, 70125, Bari, Italy
[f] Department of Engineering for Innovation, University of Salento, via per Monteroni, km 1, 73100, Lecce, Italy
[g] CEDAD - Center of Applied Physics, DAtation and Diagnostics, S.S.7 via Appia, Km 7+300, Brindisi, Italy

## ARTICLE INFO

## ABSTRACT

Boron nanoparticles (BNPs) are attractive nanomaterials for their employment in many applications, such as neutron detection, boron neutron capture therapy, proton boron capture therapy and nuclear fusion. Depending on the specific application, $^{10}$B or $^{11}$B isotopes can be used.

Nevertheless, there are significant challenges in developing suitable BNPs using both conventional chemical synthesis routes and dry fabrication techniques. In this study we report BNPs directly synthetised in water by pulsed Laser Ablation in Liquid (PLAL). Nanoparticles of elemental boron have been generated by laser ablation of a sintered $^{10}$B target in MilliQ water by employing ns laser pulse. The ablation resulted in BNPs and boron target micro-fragments with hydrogen gas and boric acid as by-products. Simple washing steps were used to obtain clean BNPs in water. The BNPs showed a narrow size distribution between 3 and 4 nm and their stability in water was induced by a thin layer of boron oxide surrounds BNPs. The BNPs were fully characterized by the chemical and structural point of view employing several techniques. A discussion on boron chemical reactions during laser ablation in water and after the NPs were released in solution was done.

## 1. Introduction

Boron and its isotopes and compounds are strategic materials for different demanding applications. Depending on the specific application, $^{10}$B or $^{11}$B isotopes can be used [1–3].

The interest towards $^{11}$B is emerging for controlled nuclear fusion energy generation [4,5] thanks to the proton Boron (pB) fusion reaction ($11B(p,\alpha)2\alpha$). The interest of such fusion reaction lies in its aneutronic nature and high yield of α particles.

For this purpose B-containing target and in particular B nanoparticles (BNPs) embedded in aerogels or polymers are of great interest [6].

The utilization of B fusion reaction presents also an opportunity to serve as a valuable and high-intensity secondary source of α particles for several applications, employing compact and cost-effective methods. One notable application is the Proton Boron Capture Therapy (PBCT), which involves the introduction of a boron solution into deep-seated tumours before irradiation with clinical proton beams, thereby enhancing the biological effectiveness of proton therapy [1,2].

Additionally, α particle sources hold promise in the production of medical radioisotopes, contributing to imaging, therapy, and theranostics [1,7].

The $^{10}$B isotope holds significant importance across various applications. Recently, it has garnered substantial attention as a conversion material in thermal neutron detectors. This increased interest arises from the escalating cost and difficulty in obtaining the widely-used converter material, $^{3}$He [8]. In light of these challenges, $^{10}$B is

---

emerging as a promising alternative due to its high capture cross-section [9]. As detection efficiency stands as a fundamental parameter for a neutron detector, numerous strategies are under consideration to enhance this metric. [10]. The most promising method appears to involve considering 3D geometries. In this regard, $^{10}$B nanoparticles are particularly noteworthy, as they aid in filling radiation-sensitive volumes [11]. In ref [12] it is reported, for example, the use of $^{10}$B nano/microparticles in order to fill microstructures of deep trenches fabricated in n-type Si (1 1 0) bulk wafers for the development of solid-state thermal neutron detectors. This approach achieved a detection efficiency of 32.2 ± 1.5 % under a self-biased condition. Moreover, in another study, Amaro et al. introduced a novel concept for neutron detection by filling a proportional counter with a $^{10}$B nanoparticle aerosol [13].

Beyond its applications in thermal neutron detection, the $^{10}$B isotope shows promise in neutron capture therapy (BNCT) [14]. BNCT is a therapeutic approach for treating tumors by selectively destroying cancer cells, leveraging the high linear energy transfer (LET) of the reaction products following neutron capture [15,16].

However, the need for a high concentration of either $^{11}$B or $^{10}$B (for PBCT and BNCT respectively), as required for effective treatments [17], raises concerns regarding toxicity when using molecular boron compounds. To address this challenge, boron-based nanoparticles offer a greater number of boron atoms, thereby improving therapeutic outcomes [18–22].

Furthermore, boron nanoparticles have the potential for use as contrast agents in photoacoustic imaging and as sensitizers in photothermal therapy, owing to their exceptional light absorption properties. Beyond this, in the past years, a lot of interest has been focused on sub-5 nm nanoparticles for their possible applications in the field of biomedical research. Several studies have shown that the smaller size of nanoparticles is critical to their biocompatibility and biodistribution properties [23,24]. Moreover, it should be noted that a fundamental requirement for NPs in vivo applications is their stability in aqueous media, while most sub-5 nm NPs are prepared in the non-aqueous phases and need to be transferred and stabilized in water. In this respect, our 3–4 nm BNPs are prepared and are stable in water (as it will be reported later) and, on this basis, may have potential for future applications in the biomedical field.

Nevertheless, there are significant challenges in developing suitable BNPs. For example, chemical synthesis pathways frequently entail intricate procedures, leading to the incorporation of undesirable by-products such as carbon and chlorine into the nanoparticles (NPs) [25]. The chemical synthesis of pure BNPs includes the reduction of unstable precursor with gas hydrogenation in solution [26]. The most used precursors are boron carbon-based isocyanates that are obtained after several processes in organic solvents and with low production yield [27]. Moreover, chemical synthesis is very far to be a green process and physical approaches are strongly recommended. Conversely, dry manufacturing techniques like laser pyrolysis lack precise regulation over parameters such as size, crystallinity, and aggregation characteristics, and the NPs produced using these techniques do not readily disperse in water [28,29]. In this scenario, pulsed laser ablation in liquid (PLAL) [30] represents an extremely promising approach for the production of pure BNP [31] also because it can be easily controlled the isotopic ratio of BNPs: the isotopic ratio of the target is held in the BNPs composition, meaning that $^{10}$B-enriched $^{10}$BNPs or $^{11}$B-enriched$^{11}$BNPs can be produced according to the starting target.

With PLAL a laser (ns or fs) is focused, with a certain irradiance, on a target immersed in liquid. Thanks to the peculiarity of laser induced plasma which expands against the liquid, NPs can be easily produced and released in the liquid. PLAL technique can have many advantages over conventional techniques such as the production of NPs without any kind of stabilizer for obtaining stable NPs with a high degree of purity and minimal surface contaminations. Additionally, the laser ablation method enables a control of NPs size (as for example employing further

laser fragmentation process), making it a valuable tool for developing $^{10}$B or $^{11}$BNPs for specific applications. It is important to note that the NPs production by this technique is not influenced by the isotopic nature of the B target. Despite these advantages, this technique has been only recently used for the synthesis of BNPs. Until now, only very few papers report a PLAL synthesis of BNPs.

In [31], Pastukhov et al. reported the formation of aqueous solutions of elemental crystalline BNPs with the averaged modal size of about 37 nm for biomedical applications using fs laser beams (1025 nm, 480 fs, 8 kHz, or 1030 nm, 270 fs) focused on a hot-pressed 99.5 %, natural isotopic boron target.

Aiyyzhy at al. [32] performed PLAL of a solid boron target in isopropanol in a continuous-flow cell using a ns (200 ns) ytterbium doped fiber laser at wavelength of 1060–1070 nm. The produced NPs resulted composed by boron and carbon with allotropic composition different by that one of the target. Some of them presented a graphitized carbon shell. The colloidal solution after laser ablation resulted highly inhomogeneous with a bimodal size distribution of NPs consisting of B and C: the majority of NPs were in the sub-micrometer range and only a small fraction of NPs measuring less than 100 nm. Further laser fragmentation of this suspension resulted in the formation of smaller nanoparticles with average size of 5–50 nm and with maximum of size distribution at 12 nm.

In this work, $^{10}$BNP synthesis by PLAL was done employing ns laser beam. The use of ns-PLAL in water for the production of BNPs, presents some important differences with respect to fs-PLAL already reported in [31]. First, the laser-matter interaction between ns- and fs-PLAL is very different as well as the ablation process, therefore different BNPs peculiarities are expected. The amount of ablated matter with ns-ablation is greater than the one obtained with fs-ablation and the heating of the ejected electrons by inverse Bremsstrahlung induces a warmer plasma leading to a smaller NP size [33]. Second, the use of ns-laser source presents some practical advantages in terms of cost and maintenance. In the present work, nanoparticles of elemental boron were generated by laser ablation of a sintered $^{10}$B target in deionized MilliQ water. The ablation resulted in boron fragments and BNPs. Following filtration and centrifugation, BNPs with narrow size distribution centered around 4 nm were obtained. Different techniques were employed for the BNPs characterization: UV–vis spectroscopy and Laser Induced Breakdown Spectroscopy (LIBS) for the concentration determination, Laser Doppler Electrophoresis (LDE) for ζ-potential measurement to point out the surface charge of the BNPs, Dynamic Light Scattering (DLS) and High-Resolution Transmission Electron Microscopy to determine the BNPs size distribution and the crystalline structure, Electron energy loss spectroscopy (EELS) to analyze the elemental content and distribution of BNPs, with special emphasis on the determination of the surface elemental composition. A detailed discussion on the processes undergoing during laser ablation and after the release of NPs in solution was also addressed.

## 2. Experimental

### 2.1. Set-ups

Pulsed Laser Ablation in Liquid (PLAL): The BNPs were produced by employing a NdYAG laser (Quanta System PILS-GIANT) with a pulse width of 6 ns, operating with wavelength of 1064 nm, repetition rate of 10 Hz and laser fluence of 64 J/cm$^2$ (laser spot diameter, 1 ± 0.2 mm). A plano convex lens of 5 cm focal length for laser focusing was used. A target of $^{10}$B (see next section) was placed on the bottom of a backer filled with 25 ml of MilliQ water. The laser ablation time was set to 2 h. The target was constantly moved (each 5 min) with a micrometer movement system during the laser ablation. A sketch and a photo of the PLAL set-up are reported in Fig. 1 During the ablation the production of BNPs was controlled by monitoring the UV–vis spectrum.

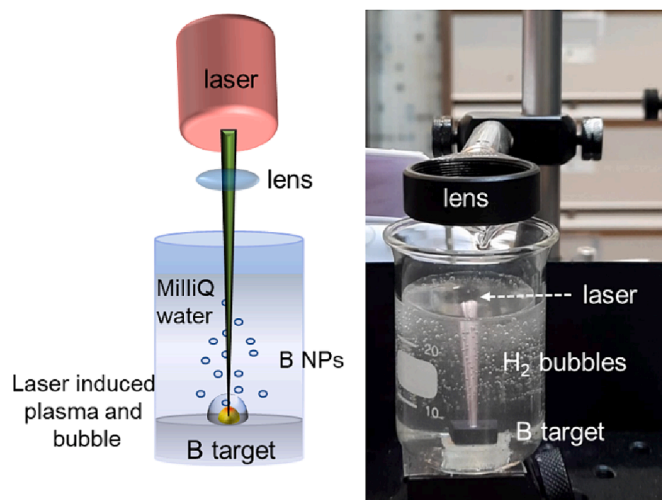Laser Induced Breakdown Spectroscopy (LIBS): The LIBS

**Fig. 1.** Sketch and photo of PLAL experimental set-up.

experiments for the quantification of produced BNPs were performed by using a Nd:YAG laser, Quantel Q-smart 850, with a pulse duration of 6 ns operating at 1064 nm. An echelle spectrometer (Aryelle 200, LTB, Germany) coupled with an ICCD (New iStar, Andor) was used for analysing plasma emission light. A biconvex lens with a focal length of 7 cm collected and focused the plasma emission on the optical fiber connected with the spectrometer. A delay time from the laser shot of 1 μs and gate width of 5 μs were used for the LIBS integrated measurements. Fig S1 shows the LIBS experimental set-up.

The experiment consists on inducing a first crater (diameter: 2.4 ± 0.2 mm) on an inert support (high pure silicon target) with a laser pulse energy of 436 mJ. Then 1 μl of purified BNPs solution was drop and dried in order to cover the whole induced crater. A laser shot of 160 mJ was finally fired for inducing plasma on the center of the crater previously formed and covered with the BNPs solution. The second laser induced crater diameter was 1.1 ± 0.2 mm, as shown in Fig.S2.

Two aligned flip-flop mountings with two different focusing lenses were used to focus the laser beam on the target: one lens with 10 cm focal length was used for 1 laser pre-shot, the other lens of 5 cm focal length was used for LIBS. In both cases, the focusing plane was set inside the target in order to obtain the desired crater diameter. All the spectra were acquired in single shot mode and each measurement was repeated 4 times (on 4 different laser induced craters, covered by BNPs solution) and then averaged. To quantify the boron of the produced BNPs, a calibration curve was previously built by using different solutions with known concentrations of $H_3BO_3$, starting from a $H_3BO_3$ mother solution 0.402 M. Each boric acid solution with known concentration was analysed in the same experimental conditions employed for the BNPs. The emission peak chosen for the analysis was B I at 249.77 nm. All the emission peaks were normalized to the background of the emission spectrum.

UV–vis spectroscopy: During laser ablation, the UV–vis spectra were acquired with an Ocean Optics (USB2000 + XR) spectrometer coupled with a light source (Mini Deuterium Halogen Light Source DT-Mini-2-GS).

The UV–vis spectra of the BNPs solution before and after purification in the region between 220 and 800 nm were registered using an Agilent 8453 UV–vis diode-array and a quartz cuvette.

Dynamic Light Scattering (DLS) and Laser Doppler Electrophoresis (LDE). DLS measurements were performed using a Zetasizer-Nano ZS from Malvern that was equipped with a 4 mW He-Ne laser ($\lambda = 633$ nm), operating at a fixed detector angle of 173° (non-invasive backscattering geometry NIBSTM) and with the cell holder maintained at 25 °C by means of a Peltier element. At least three measurements were acquired for each sample, and each reading was composed of 12 runs. The

intensity-weighted size distribution was retrieved from the field auto-correlation function by inverse Laplace transformation, using a non-negative least squares algorithm (Multiple Narrow Modes) implemented by the manufacturer. The number-weighted size distribution was evaluated from the intensity weighted size distribution, considering the vesicle form factor as detailed in ref [34]. The LDE measurements were performed (with the Zetasizer-Nano ZS) at the stationary levels of a capillary cell and the scattered light was collected in forward scattering at a fixed detector angle of 17°; the average electrophoretic mobility was retrieved with a fast field reversal sequence (high frequency alternating electric field) while the distribution of electrophoretic mobilities was obtained using slow electric field reversal sequence [35]. The ζ-potential was subsequently evaluated from the electrophoretic mobility according to the Hückel approximation. Each sample was measured 3 times and each measurement consisted of a variable number of up to 100 acquisitions.

Combination of Transmission Electron Microspy (TEM) with Energy-Dispersive X-ray Spectroscopy (EDS) and Electron Energy Loss Spectroscopy (EELS). Conventional TEM images and electron diffraction patterns were taken using a Hitachi 7700 transmission electron microscope operated at 100 kV. Whereas EELS spectra and High Resolution TEM image were recorded by a Jeol JEM-ARM 200F NEOARM operated at 200 kV. Specimens for TEM observations were prepared by drop-casting of freshly prepared solutions containing BNPs onto standard carbon supported 600-mesh copper grid and drying slowly in air naturally. Electron diffraction patterns were analyzed within the Digital Micrograph (Gatan) software package using the PASAD plug-in [36]. The software allowed a quantitative analysis of the SAED (selected area electron diffraction) patterns. It enabled to define the center of the diffraction pattern refining it at the sub-pixel resolution. In addition, elliptical distortions were also corrected. Then, the SAED patterns were transformed into electron diffraction profiles by the azimuthal integration. The background of the electron diffraction profile was subtracted by a spline fit. The software ensured reproducibility by automatically locating spline points, detecting and pre-fitting peaks. TEM images were processed by Image Pro-Plus software, in particular, the nanoparticles size distribution was determined by digitalized TEM images, performed onto 50 randomly chosen fields.

Gas chromatography (GC): Gas mixtures were analyzed using a GC (Thermo Scientific Focus GC), equipped with a SUPELCO Carboxen™ 1010 PLOT (30 m × 0.32 mm) and with a TCD detector. The analysis conditions were set as follows: a) injector temperature: 110 °C, split mode, split flow 15 mL/min, split ratio: 50; b) oven temperature: isotherm at 37 °C; c) carrier: argon 0.3 mL/min; d) detector temperature: 150 °C; e) injection volume: 1 mL.

### 2.2. Material and methods

B target for PLAL: a commercial 95 % enriched $^{10}B$ high purity (99.9 %) B sintered target, obtained from the American Elements Company in the USA was used. The target was shaped into an 8 mm × 8 mm square and then inserted at the bottom of a dedicated backer filled with MilliQ water.

Purification of produced BNPs: after the BNPs production by PLAL, the solution was transferred in a falcon container. After two days, most of the micro-fragments coming from the target damaged during the laser ablation, were in part deposited by gravity on the bottom of the target. The solution was therefore separated from the precipitate and further filtered (CA-syringe filter, Diameter: 13 mm, pore size 220 nm), to make sure that all target fragments were taken off.

During the production of BNPs, a certain quantity of $H_3BO_3$ was also produced (see the next paragraph). In order to separate BNPs from the excess of boric acid formed during ablation, the "filtered" BNP solution was subjected to three subsequent ultracentrifugation (UC) steps, performed at 45000 rpm for 2 h (using an Optima XE 90 Ultracentrifuge with a 50.2 Ti fixed-angle rotor, Beckman). After the first UC, the pellet

was collected, resuspended in a small volume of milliQ water and sonicated for 5 min in a sonicator bath. Then, the supernatant was subjected to a second UC under the same conditions. After this, the second pellet was resuspended, sonicated and mixed with the first one, while the supernatant was subjected to the third centrifugation. The third pellet was resuspended, sonicated and then mixed with the first two. This procedure allowed almost all of the particles produced by ablation to be recovered in the overall pellet in water. The particle size contained in the overall pellet was measured at DLS.

This BNPs procedure was required to ensure that LIBS measurements quantified only boron belonging to BNPs.

## 3. Results

### 3.1. Synthesis and characterization

The BNPs were directly produced in milliQ water with PLAL. During the laser ablation the Uv–vis spectrum of the colloidal solution was acquired to directly follow the formation of BNPs in solution. Fig. 2a shows the typical UV–vis spectrum of BNPs colloidal solution at different laser ablation times. In the UV–vis spectrum the optical density is plotted as a function of wavelength. When the scattering contribution to the total extinction can be neglected, as in the case of spherical NPs smaller than 30 nm [37] (such as those produced in this work) the optical density spectrum can be simply considered as an absorbance spectrum and consequently can be employed for the determination of the colloidal solution concentration. Fig. 2b shows the growth of the absorbance signal at 300 nm as a function of laser ablation time. As it is well known, the absorbance is directly linked to the concentration of the colloidal solution so from Fig. 2b it is clearly evident the growth of the BNPs concentration with the increasing of the laser ablation time. The absorbance at 300 nm was chosen because this is the wavelength after which no more absorbance by $H_3BO_3$ is revealed (see Fig. S3) and because the absorbance at 300 nm is high enough to be detected even for low concentrations of BNPs. As already reported in [32], from Fig. 2b it is evident how, even if the BNPs concentration increases with the increasing of the laser ablation time, a not perfectly linear behaviour can be found. The reason is due to the absorption of laser irradiation by the already formed colloidal solution, which leads to a decrease in laser fluence on the target surface as the concentration of BNPs increases. During the laser ablation a large production of small bubbles was always observed, as shown in Fig. 1, that we ascribed to $H_2$ gas formed during the interaction of BNP with water, as explained in the next section [38,39,28]. This last phenomenon greatly reduces the efficiency of laser ablation of B target too and consequently the yield of the BNPs with respect to that obtained when a noble metal target is irradiated.

After laser ablation, the BNPs solution showed the presence of some coarse material, probably produced by target damage during synthesis,

which was removed by gravity sedimentation and subsequent filtration. The BNPs in the filtered solution were dimensionally characterized by means of DLS. In Fig. 3 the number size distribution is presented showing a monomodal distribution of the Hydrodynamic Diameter ($H_d$) with a maximum centred at 18 nm. Since laser ablation of boron in water can lead to the formation of $H_3BO_3$, the BNPs solution underwent a series of ultracentrifugation (UC) steps to remove the boric acid, and the resulting pellet was resuspended in pure water. Following this procedure, the number size distribution determined by DLS on resuspended pellet particles remained the same as depicted before UC (see Fig. 3).

To verify the surface charge of the produced BNPs the ξ-potential was measured for the BNPs solution and for the BNPs solution after three UC cycles, obtaining $-34.7 \pm 2.0$ mV and $-39.0 \pm 2.5$ mV, respectively. These values, along with DLS data, confirm the high stability of the BNPs solutions before and after the purification and the validity of the purification method.

The BNPs were further characterized with TEM images. Fig. 4a presents a typical overview of nanoparticles in bright-field mode. The characteristic Z contrast allows the nanoparticles to be clearly discriminated from the supporting carbon film. More details on the nanoparticle size dispersion (diameter d in nm) are provided by the histogram, illustrated in Fig. 4b where the maximum of the distribution is located around $3.5 \pm 1.5$ nm. Few larger particles were also detected, but their number compared to the main population is small and can be neglected.
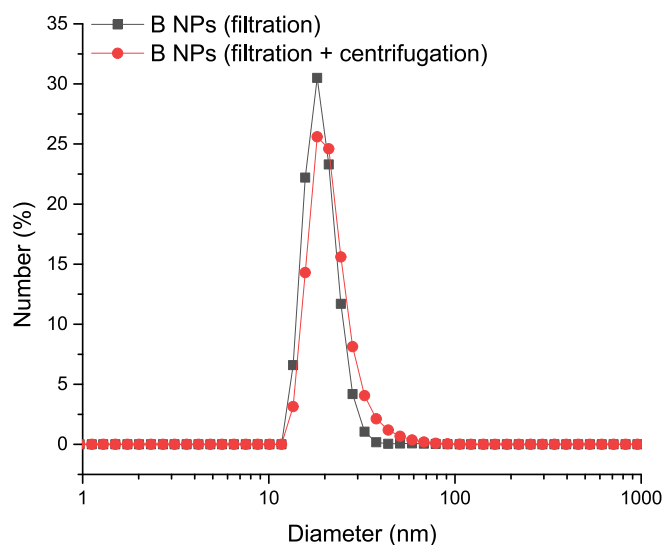
**Fig. 3.** Number size distribution of the Hydrodynamic Diameter ($H_d$) of BNP solutions before and after UC.
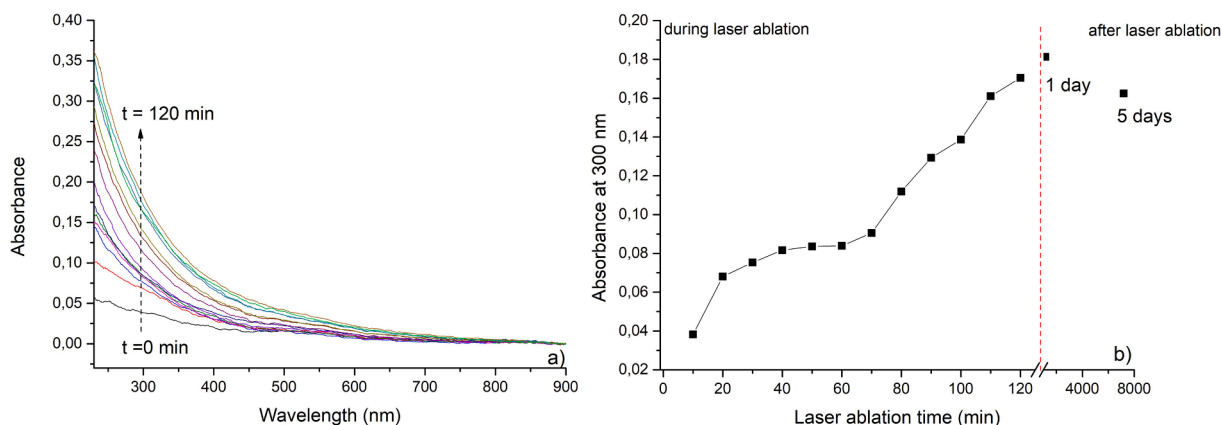
**Fig. 2.** a) UV–vis spectrum of BNPs colloidal solution at different laser ablation times and b) absorbance at 300 nm as a function of laser ablation time.
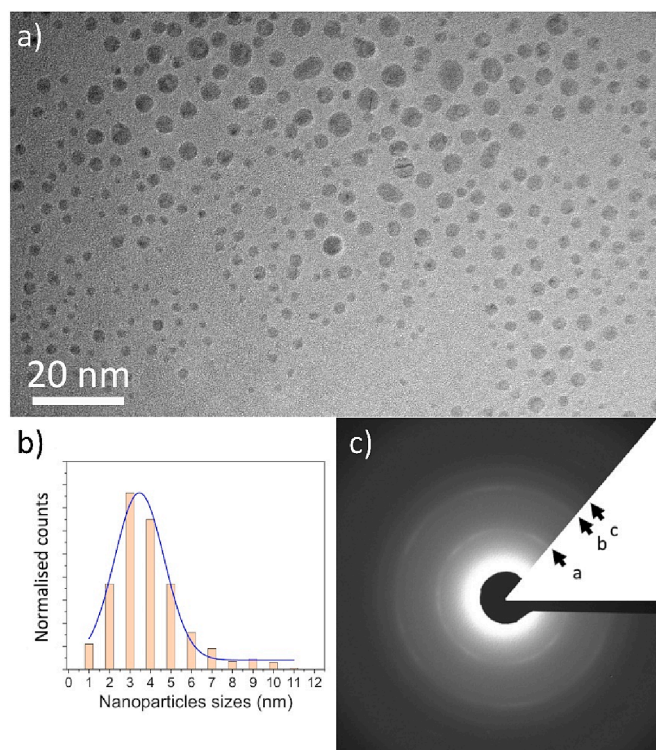
**Fig. 4.** a) Bright field image of the BNPs. b) Histogram of the nanoparticles size dispersion. c) Related diffraction pattern.

**Table 1**
Interplanar distances obtained by electron diffraction (Fig. 4c) and the corresponding label. The interplanar distances were compared with literature data for the $\alpha$ −rhombohedral boron structural modification and are in good agreement with the most intense reflections of the proposed structural modification.

| Present paper | | Literature data [42] | | |
|---|---|---|---|---|
| label | d (Å) | d (Å) | I (%) | hkl |
| | | 4.188 | 51.4 | 111 |
| a | 4.08 | 4.040 | 100 | 100 |
| b | 2.53 | 2.529 | 65.2 | 211 |
| | | 2.463 | 11.4 | 10–1 |
| c | 2.08 | 2.103 | 52.6 | 11–1 |
| | | 1.626 | 10.7 | 311 |

188.6 eV, a value that is reported in the literature as typical for $\alpha$ −r- B [43]. The value of the onset energy is a little larger than those of $\beta$ −r-B (187.8 eV) and *am*-B (187.4 eV). It can be ascribed to the fact that the band gap energy of $\alpha$ −r-B is larger than those of $\beta$-r-B and *am*-B. Indeed, theoretical calculations of the electronic structure of $\alpha$ −r-B indicate that it is a semiconductor with an indirect energy gap [44].

Also visible in the spectrum are additional components at about 191, 195 and 202 eV that can be attributed to the low dimensionality of icosahedral clusters in $\alpha$ −r-B nanocrystals [45].

Fig. 6 shows the TEM image a) together with the energy filtered image of boron b), oxygen c) and the composite image d) of a typical region of boron nanoparticles. From Fig. 6d it is clearly visible how the oxygen surrounds the surface of the BNPs.

The quantification of produced BNPs was obtained measuring their boron content by LIBS, a technique based on laser-induced plasma on samples. In the present case the BNPs solution was drop and dried on a silicon substrate as described in previous section and a focused laser shot on it was then used to produce plasma. The plasma emission was finally employed both to identify the sample elements and to perform quantitative analysis by optical emission spectroscopy. It is known that ablation of boron target also induces the formation of boric acid as by-product [31] that can bias the quantification of BNPs by LIBS. In order to avoid a BNPs overestimation, a washing procedure of synthesized BNPs based on three ultracentrifugation steps was performed in order to obtain BNPs redispersed in a pure water solution. The washing procedure does not reduce the BNP concentration, as shown in Fig. S3 where overlapped absorption spectra of NPs before and after washing steps are reported.

Fig. 7a shows a portion of LIBS emission spectra of BNPs before and after the washing steps. The B I emission lines are clearly visible along with Si I emission peaks, due to the Si of the inert substrate used for LIBS measurements. The B I emission lines intensity of BNPs before washing is higher than that of BNPs after washing. This is due to the presence of $H_3BO_3$ produced during ablation and removed by the washing procedure. In order to determine the B content in the BNPs dispersed in the pure water solution, a calibration curve was developed by performing LIBS on progressive dilutions of a $H_3BO_3$ solution at known concentration (0.402 M), the employed emission peak was B I at 249.77 nm. The LIBS emission spectrum of this solution is shown in Fig. 7b as a representative spectrum of $H_3BO_3$, while the obtained calibration curve is shown in Fig. 7b.

It can be emphasized that the coupling effect between of the surface plasmon of NPs deposited on a dielectric surface and the electromagnetic field of the laser beam is negligible, as demonstrated in [46].

The obtained B concentration for the BNPs solution was 0.00273 M (B mol /L) or 0.0295 g/L. Once the molar concentration of B belonging to the colloidal solution is known, the BNPs concentration in terms of particle for liter or mol of NPs for liter can be calculated if the size of the NPs is measured. From the TEM measurements the averaged size of the produced BNPs is 3.5 ± 1.5 nm, therefore the concentration of the produced BNPs was $8.8*10^{-7}$M (BNPs mol/L) or $5.34*10^{17}$ (n° of BNPs/ L). BNPs productivity per hour and per pulse as obtained from the mass

DLS measurements on the same BNPs sample resulted in an average $H_d$ of about 18–20 nm, which is significantly larger than that provided by TEM analysis, which reports the predominant presence of particles with an average diameter of 3–4 nm along with larger particles, as shown in Fig. 4. It should be stressed that, when particles of different sizes are present in solution, the experimental autocorrelation function (ACF) measured by DLS accounts for the light scattered by all the particles. The contributions to the ACF depend on the intensity of scattered light that scales as the sixth power of the size [40]. In the present case, the small particles mainly shown by TEM have radii around 3.5 nm and should scatter $(20/3.5)^6 \sim 34000$ times less than the large ones measured in DLS (size ∼ 20 nm). Accordingly, the contribution of very small particles to the ACF is negligible and their presence cannot be evidenced by DLS. Moreover, it should be noted that, in addition to small particles forming most of population, the presence in solution of a certain number of small aggregates cannot be excluded, thus contributing to the larger $H_d$ found by DLS.

Fig. 4c shows the selected area electron diffraction (SAED) pattern corresponding to the previously discussed image area. The continuous rings observed in the diffraction pattern are in line with the expected behavior of nanoparticles with random orientations. Boron forms four allotropes: $\alpha$-rhombohedral boron ($\alpha$ −r- B), $\alpha$ −tetragonal boron, $\beta$-rhombohedral boron ($\beta$-r-B), and $\beta$-tetragonal boron. These allotropes and amorphous boron (*am*-B) are constructed by $B_{12}$ icosahedral clusters [41]. In our case, the obtained interplanar spacings are in good agreement with the $\alpha$ −rhombohedral boron ($\alpha$-r- B), as resumed in Table 1.

Fig. 5a shows the EELS spectrum in the 150–600 eV region, acquired over an area of about 30 nm × 30 nm with an energy resolution of 0.15 eV. One can see as very pronounced the K-edge of boron at about 188 eV, the K-edge of carbon at about 284 eV, and, with much less intensity, just hinted at the K-edge of oxygen at 532 eV. In contrast, Fig. 5b shows the EELS spectrum limited to the energy range between 185 and 200 eV, a spectrum acquired with the same energy resolution of 0.15 eV. This spectral magnification allows us to better highlight the threshold characteristics of the boron edge. As is clearly visible, the onset is about
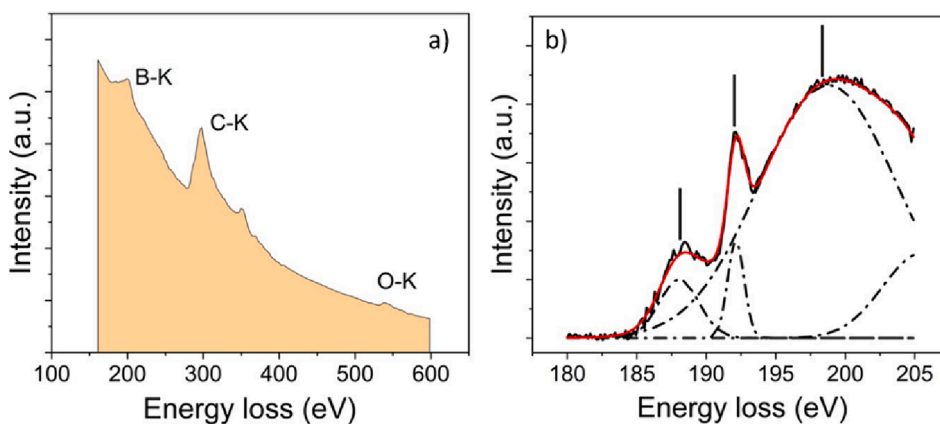
**Fig. 5.** a) EELS spectrum in the 150–600 eV region, acquired over an area of about 30 nm x 30 nm with an energy resolution of 0.15 eV, boron, carbon and oxygen edges are evident. b) EELS spectrum limited to the energy range between 185 and 200 eV.
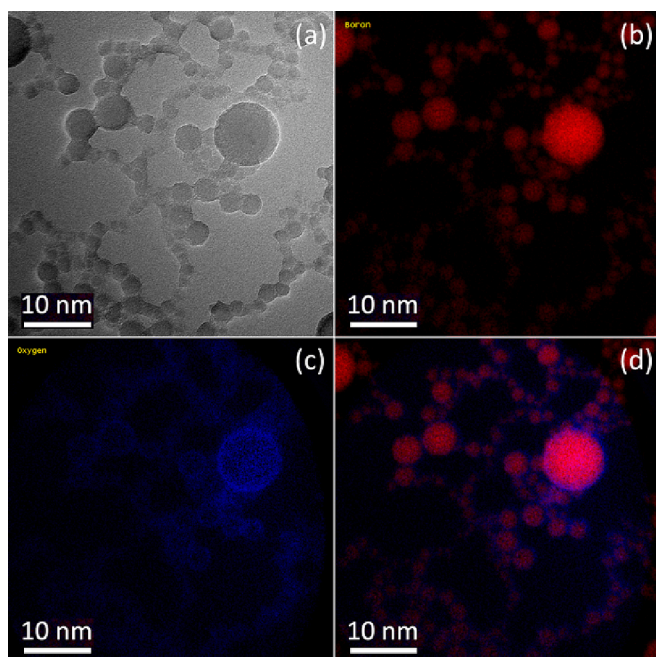


**Fig. 6.** a) TEM image of nanoparticles, b) boron map, c) oxygen map and (d) composite map (b + c) for boron and oxygen co-localization.

of the produced BNPs is reported in Table S1. The productivity is not calculated from the ablated mass because of target debris formation during NPs production, but from the mass of the produced BNPs as it was measured from UV–vis spectra after the BNPs washing.

After quantification by LIBS of BNPs, the extinction coefficient at 320 nm was determined. The UV–vis spectra of progressive dilutions of the BNPs solution (at concentration determined by LIBS) were registered and a calibration curve reporting the absorbance at 320 nm as a function of BNPs concentration constructed. Fig. S4a shows the UV–vis spectra and Fig. S4b shows the obtained calibration curve. From the Lambert-Beer law: $A = c \bullet \varepsilon \bullet l$, (where $c$ is the B concentration and $l$ is the optical path) the extinction coefficient at 320 nm has been determined as $\varepsilon_{320\ nm} = 3.43\ [(g/L)*cm]^{-1}$.

It should be taken into account that the extinction coefficient strictly depends on the NPs size, therefore the measured $\varepsilon_{320\ nm}$ is valid for BNPs with average size of 3.5 ± 1.5 nm. In Fig. S5 this extinction coefficient was employed for determining the BNPs concentration in terms of boron atomic mass/liter as a function of laser ablation time.

### 3.2. Monitoring of BNPs stability after production and after different purification steps: sedimentation, filtration and centrifugation

The BNPs solutions were monitored with UV–vis spectra during the laser ablation process (every 10 min as reported in Fig. 2 and in Fig. S5) to visualize the increasing of BNPs concentration during the ablation. In Fig.S6 the spectra acquired immediately after and 3 days after the production are reported, in order to compare the behaviour of the native BNPs solution after 3 days (useful time for the sedimentation of target micro-fragments). The UV–vis spectra show exactly the same features suggesting that the produced colloidal solution holds the same concentration. After 6 days from the production, the BNPs solution was firstly separated from the sedimented target micro-fragments and then filtered. The UV–vis spectrum of filtered BNPs solution was finally monitored for three months. As it can be seen in Fig. S6, immediately after filtration a 15 % decrease of BNPs concentration was revealed with respect to the native BNPs solution, as the consequence of the fact that some particles are retained by the pore walls of the filter. After this loss of particles, except for a natural slightly decrease due to the solution aging, the BNPs hold very similar concentration up to three months according to the UV–vis spectra.

The last purification step was the BNPs centrifugation, as described in section 2.2. Fig. S3 shows how the UV–vis spectra of the BNPs solution after filtration and after centrifugation are essentially the same, suggesting that the washing procedure does not affect the BNP concentration. Fig. S7 shows a comparison between the only filtered BNPs solution with respect to the filtered and centrifuged BNPs solution in a time frame of 14 days. UV–vis spectra and DLS measurements were performed on both solutions. The UV–vis spectra do not change in the time frame of 14 days for the just filtered BNPs solution and for the filtered and centrifuged BNPs solution, meaning that the BNPs concentration is stable, at least, for 2 weeks after the purification steps. For what concern the BNPs size monitored with DLS, the filtered solution holds the same value for two weeks. The centrifuged BNPs size slightly decreased ( 5 nm) after two weeks. It is interesting to underline that after two weeks the value of DLS measurement of centrifuged solutions becomes coincident with the one of the filtered solution (as reported in Fig. 3 and as observable by comparing Fig. S7c and d). Although DLS measurements, as mentioned above, should be taken with care, this trend suggests that the distribution size needed time to reach heterogeneous equilibrium in solution and to dissolve eventual NP aggregates. This is because the centrifuged BNPs solution was obtained dissolving the precipitate pellet produced with centrifugation in water.

In the time frame of 14 days also the concentrations of B of a) filtered BNPs solution, b) filtered and centrifuged BNPs solution and c) supernatant after three UC cycles, were determined with LIBS measurements. B concentration in the filtered BNPs solution was given by B atoms of
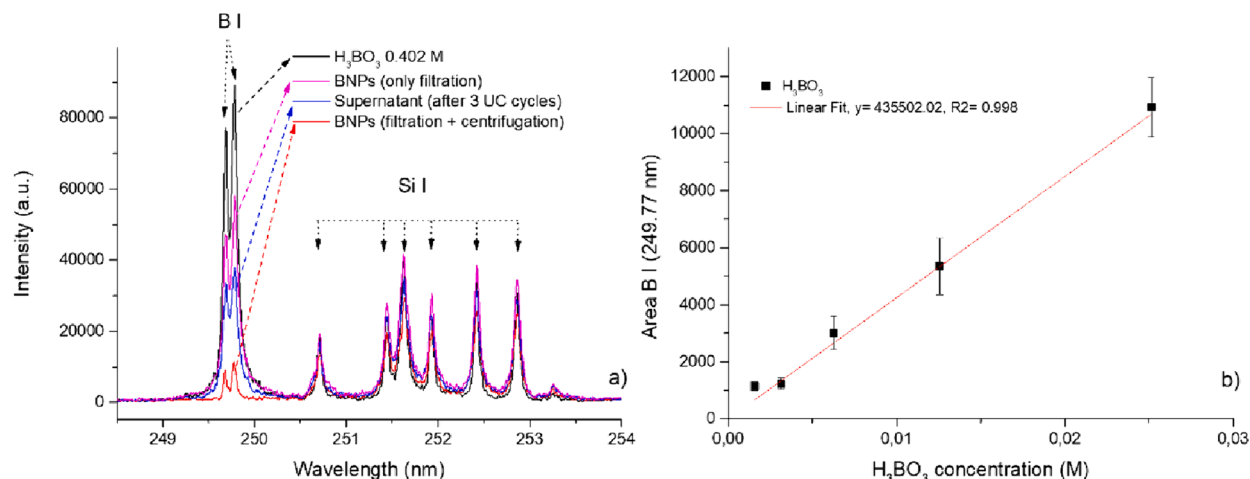
**Fig. 7.** A) portion of the libs emission spectrum and b) calibration curve for boron determination by libs.

BNPs and H$_3$BO$_3$, the B concentration in the filtered and centrifuged BNPs solution was given by B atoms of BNPs and the B concentration in the supernatant after three UC was given by B atoms of H$_3$BO$_3$. The supernatant after 3 UC contains the whole produced boric acid, since after each UC, the relative supernatant was further centrifuged. Moreover, the final water volume employed for the pellet resuspension was the same as the first BNPs solution in order to restore the concentration of the native BNPs as produced. Fig. 7a shows a frame of the LIBS emission spectra of the solutions described above where it is clearly visible the different B I intensities for each measured solution. By employing the calibration curve reported in Fig. 7b it was possible to calculate the B concentration in different solutions, as it is reported in Table 2.

In the frame of 14 days, no significant differences can be revealed in the B concentration measured in the three solutions.

Some considerations can be done.

A) By the inspection of UV–vis spectra (Fig. S7) and LIBS measurements (Table 2), both acquired in the time interval of 14 days, no significant dissolution of BNPs in water, once they are separated from boric acid, was revealed. As a matter of fact, the UV–vis spectra are able to detect only BNPs and they are not changed during 14 days and the corresponding LIBS measurements confirm the same value of B concentration within the same interval of time. Of course, it cannot be excluded further dissolution over the following months, but the BNPs can be easily stored when they are only filtered (Fig. S6) and then centrifugation step can be done when necessary.

B) The sum of the B concentration in the supernatant and the one in filtered and centrifuged BNPs solution holds the same value,

within the error of measurement, obtained for the filtered BNPs solution, meaning that with the centrifugation step there is no significant loss of B.

C) The ratio of B belonging to BNPs and B belonging to boric acid is 0.2. This value shows the ratio between boron atoms in NP phase and boron in boric acid. This ratio increases of 15 % taking into account the slightly loss of BNPs due to the filtration. The measured value is lower than that reported in ref [31] where fs-laser was employed. This observation is consistent with the fact that with ns-PLAL a high number of particles is produced (see Table S1) with very small size which have therefore a relative larger surface area when compared to the same amount of material made up of bigger particles. Since smaller NPs expose a total surface area higher than that exposed in the colloidal solution containing bigger NPs (as the case of ref. [31]), a larger number of superficial B atoms can be undergone to oxidation, therefore the boric acid produced by the oxidation process of eq.2 (see further paragraph) can have higher concentration. However the ratio discussed above can be increased by degassing the water with Argon gas during laser ablation as performed in ref. 31, or by increasing the laser ablation time, or by preparing a dedicated chamber to reduce the produced gas interaction with the laser beam with a consequent increasing of the yield.

### 3.3. Discussion

According to previous studies [47], we suppose that the nucleation and growth of the BNPs occur initially in the plasma phase. Due to the confinement effect of the water and to the cavitation compression, the plasma holds high density and temperature in the range of 5000 K. These conditions induce the formation of atomic clusters acting like seeds for the growth process as already demonstrated in ref.[33]. In this stage we do not expect any relevant difference with respect to the formation of AuNPs or CNPs, that is the releasing in solution of the NPs composed by target elements. What is clearly different is the chemistry involved after the releasing of the particle in solution. We have demonstrated that the excess of electrons in the plasma phase during ns ablation, plays an important role in the stabilization of AuNPs and in preventing the surface oxidation of the particle itself. In the case of BNPs a clear evidence of surface oxidation is shown in the HR-TEM analysis. Boron has an effective nuclear charge notably smaller than gold (2.42 and 10.9 respectively [48]), strongly reducing the BNPs electron affinity with respect to the gold ones. Moreover, while gold has a high reduction potential (+1.7 V), boron presents a negative potential in presence of water according to the following equation:

$$B + 3H_2O = H_3BO_3 + 3H^+ \ (E = -0.87 \ V) \ (1).$$

**Table 2**
B concentration of centrifuged BNPs solution, supernatant after three UC cycles and filtered BNPs solution determined by LIBS measurements in the frame of 14 days.
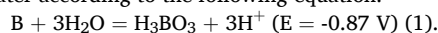
| Solutions | First LIBS measurement | Second LIBS measurement after 14 days |
|---|---|---|
| | B (g/L) | B (g/L) |
| BNPs (filtration + centrifugation) (only BNPs) | 0.023 ± 0.005 | 0.029 ± 0.007 |
| Supernatant after 3UC (only H$_3$BO$_3$) | 0.16 ± 0.04 | 0.15 ± 0.04 |
| BNPs (filtration) (BNPs + H$_3$BO$_3$) | 0.20 ± 0.05 | 0.186 ± 0.006 |

This peculiarity induces a redox reaction on the BNP surface where boron oxidizes and hydrogen reduces according to the following equation:

$$B + 3H_2O = H_3BO_3 + 3/2 \, H_2 \quad (\Delta G° = -251.865 \, KJ/mol) \quad (2).$$
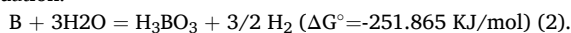
This agrees with the experimental observation where the production of small bubble of $H_2$ is noted a few seconds after the start of the process. The delay in the appearance of the bubbles implies that the oxidation process of the BNPs occurs after the release of the bubbles. On the other hand, at the plasma temperature of 5000 K the reaction in eq.2 is strongly inhibited due to the temperature-dependent equilibrium constant. Therefore, it can be expected that the oxidation process occurs after the release of the BNPs in water. In order to confirm this observation PLAL on Au and B target was performed in a sealed reactor, as it is shown in Fig. S8, and the formed gas was collected and analysed with gas chromatography. The result is shown in Fig. 8. By the inspection of the figure, we can see that while the air peak is very similar, demonstrating we sampled the same amount of gas, the $H_2$ peak is present only in the PLAL experiment with B, while in the case of Au the peak is absent or at least negligible.

The formation of the boric hydroxyl, from one hand passivates the particle surface and prevents the complete dissolution of the particle [31] with the formation of boric acid and, from the other hand stabilizes the particle. Besides this, in [32] it was supposed the boranes formation during the laser ablation on B target in water.

Previously, BNPs were produced at similar experimental conditions but with fs-laser ablation. Comparing our results with those reported in ref [31] we can observe the typical difference of the ns-PLAL and fs-PLAL. In the case of ns-PLAL higher mass removal per laser-pulse is obtained inducing a larger plasma with a duration of a few microseconds. Moreover, as a consequence of the direct absorption of the laser photons by free electrons with the inverse bremsstrahlung mechanism [49], the plasma reaches higher excitation temperature than in fs-PLAL. In ns-PLAL the particle size is determined by the growth process driven by electrostatic force (electron charged seeds attracting ions) and the surface thermal evaporation process due to the high temperature in the plasma [33]. This means that higher is the temperature, smaller is the final size of the particle. This last observation followed by the

fragmentation occurring because of subsequent laser pulses (the laser ablation time was 2 h) as well as the consuming of external layer of the BNPs surface for the boric acid formation may provide explanations for the differences in BNP size between the present work (approximately 3.5 nm) and the BNPs produced by fs-PLAL, which exhibit the peak of the size distribution at around 40 nm in diameter.

This is therefore the behaviour revealed for the [10]B-enriched [10]BNPs as produced in this paper. For other B isotopes, [11]B-enriched or [nat]B (natural isotopic ratio), being B atom characterized by light weight, tenuous isotopic effect on crystallization and reactivity should be considered. As an example, in ref. [50] slightly higher chemical activity of [10]B with respect to [nat]B during the oxidation has been reported, suggesting that [10]BNP may be more exposed to surface oxidation and consequent boric acid formation when BNPs are released in water after ablation. However, the experiments reported here, as well as those reported in Refs [31,32] confirm that, although the isotopic effect may slightly affect the formation of byproducts, PLAL is a promising method for the production of BNP with any isotopic composition equal to the isotopic composition of the target. As a matter of fact, ref. [51] by employing LAMIS (Laser Ablation Molecular Isotopic Spectrometry) technique demonstrated how the isotopic ratio of B target was held in plasma phase after ns-laser ablation.

## 4. Conclusion

In this paper the use of PLAL for the production of [10]B-enriched [10]BNPs with ns-laser ablation has been investigated. According to the experimental observation crystalline and polycrystalline NPs have been obtained with an average size of 3–5 nm. The size of the produced BNPs is much smaller than the one generally observed with PLAL process on noble metal target (about 10–20 nm). According to the redox reactions occurring with boron and water, we mainly ascribe this characteristic size to the formation of boric acid and hydrogen during the releasing of the NP in solution. From one hand the oxidation of boron with water leads to the formation of boric acid and consequently consumes the external layers of the NP, from the other hand it passivates the NP surface allowing for the stability of the NP. Moreover, also the
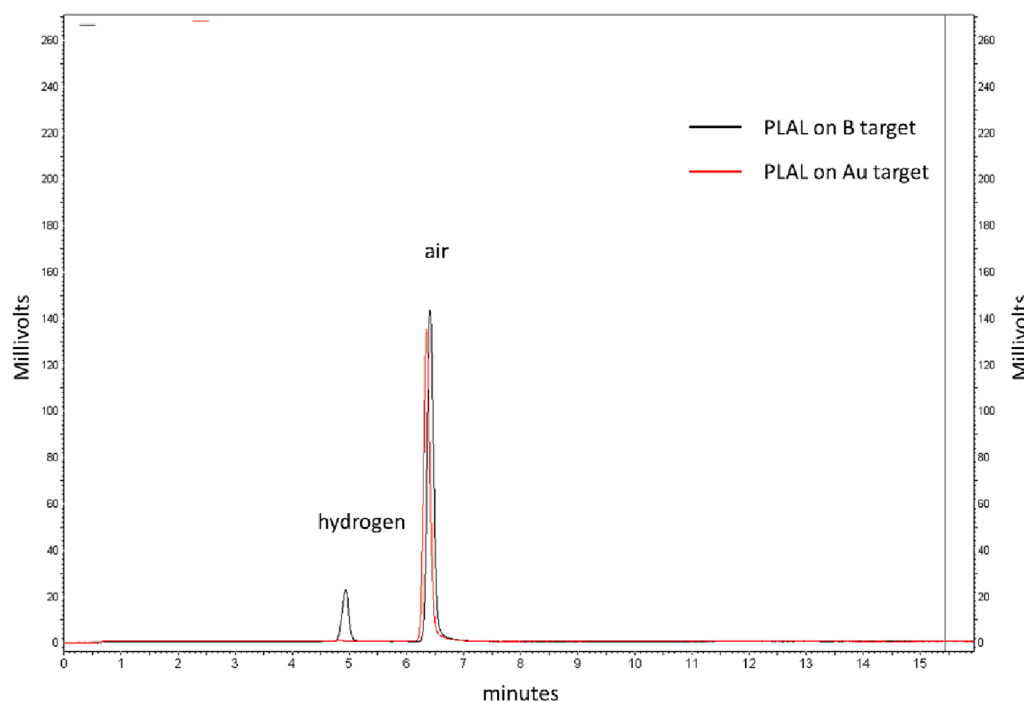


**Fig. 8.** Gas-chromatographic analysis with TCD detector of two gas samples collected during PLAL on B and Au target, respectively. The experimental conditions employed for both PLAL experiments are the same of those described in the set-up section except for the ablation time that was set to 1 h.

fragmentation occurring during an extended ablation time contributes to obtaining such a small size. In this study the feasibility of ns-PLAL for the production of BNPs with an NPs productivity of 0.4 mg h$^{-1}$, 0.01 μg pulse$^{-1}$ corresponding to $1.9*10^{11}$n$°$ BNPs pulse$^{-1}$ has been shown, taking in mind the employment of ns-laser with low repetition rate (10 Hz) and a low laser ablation time (2 h). The quantification of produced boric acid as well as the easy purification steps of BNPs from by-products were also shown. The limited production in g/L is attributed to the efficient formation of the boric acid and the generation of a large quantity of H$_2$ bubbles that scatter the incoming laser pulses, reducing the effective laser energy on the target. Whitin this context, the need for suitable reactor designs arises to enhance the yield of BNPs. However, this observation also attests to the potential use of laser ablation on boron as a promising tool for H$_2$ production.

## CRediT authorship contribution statement

**Marcella Dell'Aglio:** Writing – review & editing, Writing – original draft, Supervision, Methodology, Investigation, Formal analysis, Data curation, Conceptualization. **Alessandro De Giacomo:** Writing – review & editing, Writing – original draft, Validation, Supervision, Methodology, Investigation, Formal analysis, Data curation, Conceptualization. **Daniela Manno:** Data curation, Formal analysis, Writing – original draft. **Antonia Mallardi:** Formal analysis, Methodology, Writing – original draft, Data curation. **Chiara Provenzano:** Data curation, Formal analysis, Validation. **Marcella Marra:** Data curation, Formal analysis, Validation. **Francesco Nocito:** Investigation, Formal analysis, Data curation. **Antonio Serra:** Validation, Methodology, Investigation, Data curation. **Gianluca Quarta:** Investigation, Formal analysis, Data curation. **Anna Paola Caricato:** Writing – original draft, Validation, Supervision, Methodology, Conceptualization.

## Declaration of competing interest

The authors declare that they have no known competing financial interests or personal relationships that could have appeared to influence the work reported in this paper.

## Data availability

No data was used for the research described in the article.

## Acknowledgements

## Appendix A. Supplementary data

Supplementary data to this article can be found online at https://doi.org/10.1016/j.apsusc.2024.160089.

## References

[1] P. Bláha, C. Feoli, S. Agosteo, M. Calvaruso, F.P. Cammarata, R. Catalano, M. Ciocca, G.A.P. Cirrone, V. Conte, G. Cuttone, A. Facoetti, G.I. Forte, L. Giuffrida, G. Magro, D. Margarone, L. Minafra, G. Petringa, G. Pucci, Va. Ricciardi, E. Rosa, G. Russo, L. Manti, The proton-boron reaction increases the radiobiological effectiveness of clinical low-and high-energy proton beams: novel experimental evidence and perspectives, Front. Oncol. 11 (2021) 682647.

[2] I.N. Zavestovskaya, A.L. Popov, D.D. Kolmanovich, G.V. Tikhonowski, A. I. Pastukhov, M.S. Savinov, P.V. Shakhov, J.S. Babkova, A.A. Popov, I.V. Zelepukin, M.S. Grigoryeva, A.E. Shemyakov, S.M. Klimentov, V.A. Ryabov, P.N. Prasad, S. M. Deyev, A.V. Kabashin, Nanomaterials 13 (2023) 2167.

[3] K. Szkliniarz, M. Sitarz, R. Walczak, J. Jastrzębski, A. Bilewicz, J. Choiński, A. Jakubowski, A. Majkowska, A. Stolarz, A. Trzcińska, W. Zipper, Production of medical Sc radioisotopes with an alpha particle beam, Appl. Radiat. Isot. 118 (2016) 182–189.

[4] D.C. Moreau, Potentiality of the proton-boron fuel for controlled thermonuclear fusion, Nucl. Fusion 17 (1977) 13.

[5] H. Hora, G. Korn, L. Giuffrida, D. Margarone, A. Picciotto, J. Krasa, K. Jungwirth, J. Ullschmied, P. Lalousis, S. Eliezer, G.H. Miley, S. Moustaizis, G. Mourou, Fusion energy using avalanche increased boron reactions for block-ignition by ultrahigh power picosecond laser pulses, Laser Part. Beams 33 (2015) 607–619.

[6] K. Dale, N. Vargas, A. Jara, E. Marin, G. Lovelace, N. Langley, J. Williams, T. Reuter, C. Kong, C. Monton, N. Alexander, M. Farrell, W. Sweet, Fabricating Boron-Doped Nanowires, Fusion Science and Technology, Doi: 10.1080/15361055.2023.2169547.

[7] S. Qaim, I. Spahn, B. Scholten, B. Neumaier, Uses of alpha particles, especially in nuclear reaction studies and medical radionuclide production, Radiochim. Acta 104 (2016) 601–624.

[8] K. Zeitelhack, Search for alternative techniques to helium-3 based detectors for neutron scattering applications, Neutron News 23 (4) (2012) 10–13.

[9] A.P. Caricato, M. Cesaria, P. Finocchiaro, S. Amaducci, F. Longhitano, C. Provenzano, M. Marra, M. Martino, M.R. Aziz, A. Serra, D. Manno, L. Calcagnile, G. Quarta, Thermal neutron conversion by high purity 10B-enriched layers: PLD-growth, thickness-dependence and neutron-detection performances, Eur. Phys. J. plus 137 (2022) 431.

[10] C. Provenzano, M. Marra, Anna Paola Caricato, Paolo Finocchiaro, Simone Amaducci, Fabio Longhitano, Maurizio Martino, Gaetano Elio Poma, Gianluca Quarta, Development of a High-Efficiency Device for Thermal Neutron Detection Using a Sandwich of Two High-Purity 10B Enriched Layers, Sensors (basel) 14 (2023) 9831.

[11] R. Mendicino, M. Boscardin, S. Carturan, G.-F. Dalla Betta, M. Dalla Palma, G. Maggioni, A. Quaranta, S. Ronchin, Characterization of 3D and planar Si diodes with different neutron converter materials, Nucl. Instr. and Meth. A 796 (2015) 23–28.

[12] [Wei-Jen Chan , Sasinan Bupphathong, Han-Lin Cho, Venkanagouda S Goudar, Sina Dehestani, Chi-Shiun Chiang, Fan-Gang Tseng, Boron-10 nanoparticles filled silicon trenches for thermal neutron detection application Appl. Phys. Lett. 110 (2017) 192105 Doi: 10.1063/1.4983289].

[13] [F. D. Amaro, C. M. B. Monteiro, J. M. F. dos Santos & A. Antognini, Novel concept for neutron detection: proportional counter filled with 10B nanoparticle aerosol, Scientific Reports volume 7, (2017), Article number: 41699].

[14] T.D. Malouff, D.S. Seneviratne, D.K. Ebner, W.C. Stross, M.R. Waddle, D. M. Trifiletti, S. Krishnan, Boron neutron capture therapy: A review of clinical applications, Front. Oncol. 11 (2021) 351.

[15] M. Shanmugam, N. Kuthala, X. Kong, C.S. Chiang, K.C. Hwang, Combined Gadolinium and Boron Neutron Capture Therapies for Eradication of Head-and-Neck Tumor Using Gd(10)B(6) Nanoparticles under MRI/CT Image Guidance, JACS Au 3 (2023) 2192–2205.

[16] I.N. Zavestovskaya, A.I. Kasatova, D.A. Kasatov, J.S. Babkova, I.V. Zelepukin, K. S. Kuzmina, G.V. Tikhonowski, A.I. Pastukhov, K.O. Aiyyzhy, E.V. Barmina, A. A. Popov, I.A. Razumov, E.L. Zavjalov, M.S. Grigoryeva, S.M. Klimentov, V. A. Ryabov, S.M. Deyev, S.Y. Taskaev, A.V. Kabashin, Laser-Synthesized Elemental Boron Nanoparticles for Efficient Boron Neutron Capture Therapy, Int J Mol Sci 24 (2023).

[17] W. Sauerwein, A. Wittig, R. Moss, Y. Nakagawa, Neutron Capture Terapy: Principles and Applications, SpringerLink, 2012.

[18] I. B. Belyaeva, I. V. Zelepukina, A. I. Pastukhov, P. V. Shakhov, G. V. Tikhonowski, A. A. Popov, A. Yu. Zakharkiv, S. M. Klimentov, A. A. Garmash, I. N. Zavestovskaya, S. M. Deyeva, and A. V. Kabashin, Bulletin of the Lebedev Physics Institute, 2022, Vol. 49, No. 6, pp. 185–189. © Allerton Press, Inc., 2022.

[19] S.A. Uspenskii, P.A. Khaptakhanova, Boron nanoparticles in chemotherapy and radiotherapy: the synthesis, state-of-the-art, and prospects, Russ Chem Bull 71 (2022) 2533–2560.

[20] X. Zhang, Y. Lin, N.S. Hosmane, Y. Zhu, Nanostructured boron agents for boron neutron capture therapy: a review of recent patents, Med Rev 3 (5) (2023) 425–443.

[21] Y. Zhu, Koh Cheng Yan, John Maguire, Narayan Hosmane, Recent Developments in Boron Neutron Capture Therapy (BNCT) Driven by Nanotechnology, Current Chemical Biology 1 (2) (2007) 141–149.

[22] S. Scaramuzza, C. M.G de Faria, V. Coviello, D. Forrer, L. Artiglia, D. Badocco, P. Pastore, P. Ghigna, I. Postuma, L. Cansolino, C. Ferrari, S. Bortolussi, R. Vago, A. E. Spinelli, M. Bekić, M. Čolić, V. Amendola, A Laser Synthesis Route to Boron-Doped Gold Nanoparticles Designed for X-Ray Radiotherapy and Boron Neutron Capture Therapy, Adv. Funct. Mater. 33 (2023) 2303366.

[23] M. Xie, Y. Xu, J. Huang, Y. Li, L. Wang, L. Yang, H. Mao, Going Even Smaller: Engineering Sub-5 nm Nanoparticles for Improved Delivery, Biocompatibility and Functionality, WIREs Nanomed Nanobiotechnol. 12 (2020) e1644.

[24] Xu. Jiaqi, M. Song, Z. Fang, L. Zheng, X. Huang, K. Liu, Applications and challenges of ultra-small particle size nanoparticles in tumor therapy", Journal of Controlled Release 353 (2023) 699–712.

[25] S. Tatiya, M. Pandey, S. Bhattacharya, Nanoparticles containing boron and its compounds: Synthesis and applications: A review, J. Micromanuf. 3 (2020) 159–173.

[26] Y. Zhu, P. Prommana, Narayan S Hosmane, Paolo Coghi, Chairat Uthaipibull, Yingjun Zhang, Functionalized Boron Nanoparticles as Potential Promising Antimalarial Agents, ACS, Omega 7 (2022) 5864–5869.

[27] Y. Zhu, N.S. Hosmane, Liquid-Phase Synthesis of Boron Isocyanates: Precursors to Boron Nanoparticles, Angew. Chem., Int. Ed. 57 (2018) 14888–14890.

[28] P. Rohani, S. Kim, M.T. Swihart, Boron Nanoparticles for room-temperature hydrogen generation from water, Adv. Energy Mater. 6 (2016) 1502550.

[29] D.H. Nguyen, N.M. Chu, Y. Tokoi, T.-M.-D. Do, T. Nakayama, H. Suematsu, K. Niihara, Preparation of boron nanoparticles by pulsed discharge of compacted powder, Jpn. J. Appl. Phys. 59 (2020) SCC05.

[30] P.V. Kazakevich, A.V. Simakin, V.V. Voronov, G.A. Shafeev, Laser-induced synthesis of nanoparticles in liquids, Appl. Surf. Sci. 252 (13) (2006) 4373–4380, https://doi.org/10.1016/j.apsusc.2005.06.059.

[31] A.I. Pastukhov, I.B. Belyaev, J.C. Bulmahn, I.V. Zelepukin, A.A. Popov, I. N. Zavestovskaya, S.M. Klimentov, S.M. Deyev, P.N. Prasad, A.V. Kabashin, Laser-ablative aqueous synthesis and characterization of elemental boron nanoparticles for biomedical applications, Scientific Reports 12 (1) (2022) 9129, https://doi.org/10.1038/s41598-022-13066-8.

[32] K.O. Aiyyzhy, E.V. Barmina, V.V. Voronov, G.A. Shafeev, G.G. Novikov, O. V. Uvarov, Laser ablation and fragmentation of Boron in liquids, Optics and Laser Technology 155 (2022) 108393.

[33] Taccogna, F., Dell'Aglio, M., Rutigliano, M., Valenza, G., De Giacomo, A., On the growth mechanism of nanoparticles in plasma during pulsed laser ablation in liquids, (2017) Plasma Sources Science and Technology, 26 (4), art. no. 045002.

[34] A. Mallardi, N. Nuzziello, M. Liguori, C. Avolio, G. Palazzo, Colloids Surf. B Biointerfaces 168 (2018) 134–142.

[35] H. Mateos, A. Valentini, E. Robles, A. Brooker, N. Cioffi, G. Palazzo, Colloids Surf., A 576 (2019) 82–90.

[36] C. Gammer, C. Mangler, C. Rentenberger, H.P. Karnthaler, Quantitative local profile analysis of nanomaterials by electron diffraction, Scr. Mater. 63 (3) (2010) 312–315, https://doi.org/10.1016/j.scriptamat.2010.04.019.

[37] D. Evanoff Jr., G. Chumanov, Size-controlled synthesis of nanoparticles. 2. Measurement of extinction, scattering, and absorption cross sections, J. Phys. Chem. B 108 (2004) 13957–13962.

[38] L. Escobar-Alarcón, J.L. Iturbe-García, F. González-Zavala, D.A. Solis-Casados, R. Pérez-Hernández, E. Haro-Poniatowski, Hydrogen production by laser irradiation of metals in water under an ultrasonic field: A novel approach, International Journal of Hydrogen Energy 44 (3) (2019) 1579–1585.

[39] M.-R. Kalus, R. Lanyumba, N. Lorenzo-Parodi, M.A. Jochmann, K. Kerpen, U. Hagemann, T.C. Schmidt, S. Barcikowski, B. Gocke, Phys. Chem. Chem. Phys. 21 (2019) 18636.

[40] G. Palazzo, L. Paduano, Diffusion measuring techniques, in: D. Berti, G. Palazzo (Eds.), Colloid. Found. Nanosci., Second ed.,, Elsevier, 2021, pp. 199–231.

[41] O. A. Golicova, Phys. Stat. Sol. 101, 277 (1987) - K. Katada, Jpn. J. Appl. Phys. 5, 582 (1966) - B. F. Decker and J. S. Kasper, Acta Crystallogr. 12, 503 (1959) - D. W. Bullett, J. Phys. C 15, 415 (1982.

[42] Qi An, K. Madhav Reddy, Kelvin Y. Xie, Kevin J. Hemker, and William A. Goddard PHYSICAL REVIEW LETTERS 117, 085501 (2016).

[43] M. Terauchi, Y. Kawamata, M. Tanaka, M. Takeda, K. Kimura, Electron Energy-Loss Spectroscopy Study of the Electronic Structure of a-Rhombohedral Boron, JOURNAL OF SOLID STATE CHEMISTRY 133 (1997) 156–159.

[44] W. Bullett, J. Phys. C 15, 415 (1982) - S. Lee, D. M. Bylander, and L. Kleinman, Phys. Rev. B 42, 1316 (1990) - D. Li, Y. N. Xu, and W. Y. Ching, Phys. Rev. B 45, 5896 (1992).

[45] M. Kobayashi, J. Mater. Sci. 23 (1988) 4392.

[46] A. De Giacomo, R. Gaudiuso, C. Koral, M. Dell'Aglio, O. De Pascale, Nanoparticle Enhanced Laser Induced Breakdown Spectroscopy: Effect of nanoparticles deposited on sample surface on laser ablation and plasma emission, Spectrochimica Acta - Part B Atomic Spectroscopy 98 (2014) 19–27.

[47] Dell'Aglio, M., Motto-Ros, V., Pelascini, F., Gornushkin, I.B., De Giacomo, A.*, Investigation on the material in the plasma phase by high temporally and spectrally resolved emission imaging during pulsed laser ablation in liquid (PLAL) for NPs production and consequent considerations on NPs formation, (2019) Plasma Sources Science and Technology, 28 (8), art. no. 085017.

[48] E. Clementi, D.L. Raimondi, W.P. Reinhardt, Atomic Screening Constants from SCF Functions. II. Atoms with 37 to 86 Electrons, J. Chem. Phys. 47 (1967) 1300–1307.

[49] A. De Giacomo, M. Dell'Aglio, A. Santagata, R. Teghil, Early stage emission spectroscopy study of metallic titanium plasma induced in air by femtosecond- and nanosecond-laser pulses Spectrochimica Acta - Part B, Atomic Spectroscopy 60 (7–8) (2005) 935–947.

[50] Levan S. Chkhartishvili, Isotopic effects of boron, Trends in Inorganic Chemistry. Vol. 11, 2009.

[51] X. Mao, A. Alexander, Bol'shakov b, Dale L. Perry a, Osman Sorkhabi a, Richard E. Russo, Laser Ablation Molecular Isotopic Spectrometry: Parameter influence on boron isotope measurements, Spectrochimica Acta Part B 66 (2011) 604–609.